Build Simul (2015) 8: 405 – 414
DOI 10.1007/s12273-015-0232-9

Real-time flow simulation of indoor environments using lattice Boltzmann method

M. Amirul Islam Khan[1] (✉), Nicolas Delbosc[2], Catherine J. Noakes[1], Jonathan Summers[2]

1. School of Civil Engineering, University of Leeds, Woodhouse Lane, Leeds LS2 9JT, UK
2. School of Mechanical Engineering, University of Leeds, Woodhouse Lane, Leeds LS2 9JT, UK

Abstract

A novel lattice Boltzmann method (LBM) based 3D computational fluid dynamics (CFD) technique has been implemented on the graphics processing unit (GPU) for the purpose of simulating the indoor environment in real-time. We study the time evolution of the turbulent airflow and temperature inside a test chamber and in a simple model of a four-bed hospital room. The predicted results from LBM are compared with traditional CFD based large eddy simulations (LES). Reasonable agreement between LBM results and LES method is observed with significantly faster computational times.

Keywords

real-time,
lattice Boltzmann,
graphics processing unit,
computational fluid dynamics,
hospital room

Article History

Received: 31 October 2014
Revised: 28 April 2015
Accepted: 29 April 2015

1 Introduction

In the past few years, computational fluid dynamics (CFD) has been playing an increasingly important role in the assessment of building design (Zhai 2006). The information provided by CFD has been extensively applied to all aspects and stages of building design. CFD can provide detailed information about outdoor airflows around buildings as well as parameters in the indoor environment, such as air velocity, temperature and contaminant concentrations. CFD has been used to analyse the thermal environment (Mariani and da Silva 2007), design of ventilation systems (Asfour and Gadi 2007) and for evaluating indoor air quality (IAQ) (Zhao and Guan 2007). Furthermore, CFD methods have been used to study smoke dispersion in buildings (Qin et al. 2009) and model environment specific parameters such as airborne pathogen transport (Noakes et al. 2006) inside hospitals.

While these CFD studies yield valuable information that informs building design and operation, the majority of models consider steady-state scenarios which are not able to capture the transient effects due factors such as the movement of people, changes to heat sources or fluctuations present, particularly in naturally ventilated systems. The major constraint in developing transient models is excessive computation time (Jin et al. 2012); depending on the CFD model used the calculation time might extend from hours to months (Zuo et al. 2010). Hence, CFD based models are limited in their ability to provide quick evaluation at conceptual design stage, and in conducting risk assessments for situations such as smoke management in case of building fire and the transmission of airborne infectious contaminant spreading in hospital wards.

Researchers (Béghein et al. 2005) have attempted using supercomputers or computer clusters to accelerate the CFD simulation. Although this resulted in a significant reduction of the computation time, this approach requires large, well-managed and expensive computing facilities (Zuo and Chen 2010). Such facilities are seldom available to building designers and emergency management teams. Hence, in order to

E-mail: A.Khan@leeds.ac.uk

simulate indoor air distributions with good physical accuracy and within an acceptable computing time, it is essential to develop a method that is faster than conventional CFD while maintaining the accuracy of the results. The most popular amongst the fast computational methods for predicting indoor air distributions, faster than CFD, are multizone network models (Wang and Chen 2007) and zonal models (Megri and Haghighat 2007). These models can give a reasonable approximation of bulk parameters and the influence of key parameters but are simplistic in their assumptions and hence suffer in terms of physical accuracy. For example, multizone network models assume a uniform contaminant concentration and temperature distribution inside each zone or room and thereby cannot provide insight into the variation of these quantities present in a real room. Furthermore, these models are not easily adaptable and require special models and zones to be incorporated for every new building configuration. CFD simulations can be coupled with multizone (Wang and Chen 2007) models to improve accuracy for specific zones of interest, but at the expense of losing the advantage of fast computation time due to the CFD simulation's long computing time (Jin et al. 2012). More recently a fast fluid dynamics (FFD) method has been used to simulate indoor environments in real-time (Zuo and Chen 2009; Zuo et al. 2010). The FFD model was originally developed for creating visually appealing fluid animations in the computer games industry (Stam 1999) rather than aiming for physical accuracy. The FFD model solves the Navier–Stokes equations (NSE) based on the combination of the semi-Lagrangian and pressure projection method thereby sacrificing some accuracy (Zuo and Chen 2009). The FFD method significantly reduces computing effort but it is not as accurate as a CFD model. It can capture the overall flow features of indoor airflows and provide much more detailed information than the multizone and nodal models. The computing speed of the FFD model has been shown to be about 50 times faster than that of the CFD (Zuo and Chen 2009). Although more accurate than network and zonal models, FFD still needs further improvements to be used as an engineering tool. Recent works by Jin et al. (2012) and Zuo et al. (2010) have shown some promising outcomes.

In this work we explore the potential for using a non-traditional lattice Boltzmann method (LBM) (Chen and Doolen 1998) for indoor airflow simulation. We apply an interactive and real-time LBM CFD model with an integrated visualisation tool developed in (Delbosc et al. 2014) to evaluate the suitability, accuracy and usefulness of a 3D LBM based real-time, thermal and turbulent airflow solver running on a graphic processing unit (GPU) platform. The implementation of LBM on the GPU is not unique in the sense that traditional CFD based methods could also be implemented on the GPU (Thibault and Senocak 2009). But due to the local nature of the LBM algorithm along with the absence of any non-local Poisson pressure loop lends itself to be easily parallelisable compared to traditional CFD methodology on GPUs (Delbosc et al. 2014). Furthermore our algorithm allows turbulent flow simulation and visualisation to be performed simultaneously with real-time user interaction and computational steering on a single desktop computer (Delbosc et al. 2014). Results obtained from our computations are compared with a traditional turbulent flow solver running on multi-core central processing units (CPUs) based platform. This is initially carried out on a highly accurate lid-driven cavity benchmark problem, followed by a comparison of the computational speed and accuracy of the LBM method with traditional CFD method for a full-scale environment chamber. The study also demonstrates the application of the method to evaluating transient thermal flows in hospital scenario.

2 The LBM method for three-dimensional thermal and turbulent flow

The LBM approach is a microscopically inspired method designed to solve macroscopic fluid dynamics problems. It is at the interface between the microscopic (molecular) and macroscopic (continuum) worlds, aiming to capture the best of both. The LBM originates from the lattice gas automata (LGA) method (Frisch et al. 1986) and can be regarded as an explicit discretisation of the Boltzmann equation. The LBM has several advantages over the Navier–Stokes equations, such as its numerical stability and accuracy, the capacity to efficiently handle complex geometries and the data-parallel nature of its algorithm. Thus the LBM is an explicit numerical scheme with only local operations. It has the advantage of being easy to implement and is especially well suited for massively parallel machines like graphics processing units (GPUs) (Obrecht et al. 2012). There are few disadvantages of the LBM in comparison to the traditional CFD based method. It is currently limited to extremely low Mach number flows and the algorithm is memory intensive (Elhadidi and Khalifa 2013). LBM also uses more time steps due to the explicit nature of the scheme with advection limited step size (Elhadidi and Khalifa 2013). Furthermore implementations of the boundary conditions in LBM are nontrivial and sometimes complicated due to the fact that a single boundary condition (such as no-slip) on the macroscopic scale could be formulated with many different types of microscopic formulation (Chen and Doolen 1998). LBM has been previously used by Crouse et al. (2002) and Zhang and Lin (2010) to explore its usefulness in the indoor environment simulation. Recent claims by Elhadidi and Khalifa (2013) of a traditional CFD based coarse simulation using commercial

software Fluent to perform faster than real-time and more accurate than LBM method are questionable due to the usefulness of such a method in a real dynamic scenario.

The LBM algorithm is based on threefold discretisation of the Boltzmann equation in phase space, involving space, time and velocities. The movement and distributions of a fluid are described by particle distribution functions residing at the sites of a regular grid or lattice of points which encompasses our entire indoor environment i.e. a room for example. The particle distribution functions represent the probability of particle presence with a given velocity at each lattice site. The macroscopic quantities of the fluid like the density ρ or the velocity $\boldsymbol{v}$ can be recovered from these distribution functions. The movement of the particle population is restricted to a fixed set of directions $\boldsymbol{e}_i$ defined on the links between neighbouring sites and given for a three-dimensional lattice D3Q19 (see Fig. 1) by

$$\boldsymbol{e}_i = \begin{cases} (0,\ 0,\ 0) & i=0 \\ (\pm1,\ 0,\ 0),(0,\ \pm1,\ 0),(0,\ 0,\ \pm1) & i=1-6 \\ (\pm1,\ \pm1,\ 0) & i=7-10 \\ (\pm1,\ 0,\ \pm1) & i=11-14 \\ (0,\ \pm1,\ \pm1) & i=15-18 \end{cases}$$

The LBM is composed of two fundamental steps. In every discrete time step, distribution functions are first streamed along links from each site to their neighbouring sites (the streaming-step). Then the distribution functions are relaxed towards a local equilibrium based on the new macroscopic quantities at the site (the collision-step). While the streaming-step only depends on the lattice geometry, the collision-step encodes all the physics of the model and the chosen relaxation scheme specifies the stability and the accuracy of the method. Another important part of any LBM simulation is the implementation of the boundary conditions which takes place before or after the collision-step. Boundary conditions can be implemented in various ways in the LBM, but in principle, they define the unknown distribution functions at the boundary in order to recover the desired macroscopic equations. Full details of this approach are set out in (Delbosc et al. 2014).

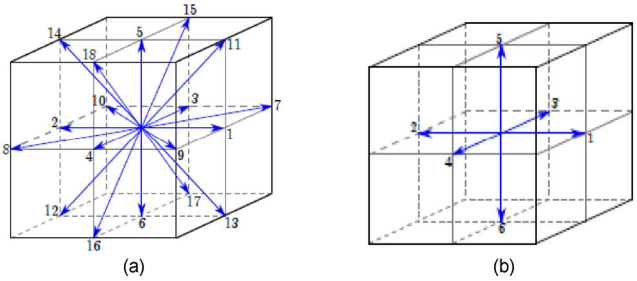

Fig. 1 Diagram of a single node in the (a) D3Q19 and (b) D3Q6 lattice respectively

2.1 The D3Q19 model

A common labelling for lattices used in LBM is DdQq; where d is the space dimension and q the number of microscopic velocities. There are several possible nodes for 3D lattices, such as D3Q13, D3Q15, D3Q19, D3Q27... The D3Q19 model, illustrated in Fig. 1(a), was chosen because it has a minimum number of velocities while maintaining good isotropy of the lattice.

The simulation of the velocity field is carried out on such a D3Q19 lattice; the complex collision operator is approximated by using the standard Bhatnagar–Gross–Krook (BGK) scheme (Bhatnagar et al. 1954) which states that the distribution functions $\boldsymbol{f} = \{f_i\}$, $i \in \{0, 1,..., 18\}$ is close to a local equilibrium $\boldsymbol{f}^{(\mathrm{eq})} = \{f_i^{(\mathrm{eq})}\}$, $i \in \{0, 1,..., 18\}$ and relaxes toward this equilibrium with some characteristic time τ. The evolution of the distribution functions using the BGK collision is described by the following equation:

$$f_i(\boldsymbol{x} + c\boldsymbol{e}_i\Delta t,\ t+\Delta t) = f_i(\boldsymbol{x},t) - \frac{1}{\tau}\left(f_i(\boldsymbol{x},t) - f_i^{(\mathrm{eq})}(\boldsymbol{x},t)\right) \tag{1}$$

where $c = \Delta x/\Delta t$ is the lattice speed, and Δx and Δt are the lattice spacing and time increment, respectively. The fluid density ρ and velocity $\boldsymbol{u}$ are determined from the zero and the first moments of the distribution functions:

$$\rho = \sum_{i=0}^{18} f_i(\boldsymbol{x},t), \quad \rho\boldsymbol{u} = \sum_{i=0}^{18} c\boldsymbol{e}_i f_i(\boldsymbol{x},t) \tag{2}$$

The local equilibrium distribution functions are computed from the new density ρ and velocity $\boldsymbol{u}$ (obtained after the streaming-step) by using the following formula:

$$f_i^{(\mathrm{eq})} = \rho w_i\left(1 + 3\frac{\boldsymbol{e}_i\cdot\boldsymbol{u}}{c} + \frac{9}{2}\frac{(\boldsymbol{e}_i\cdot\boldsymbol{u})^2}{c^2} - \frac{3}{2}\frac{\boldsymbol{u}^2}{c^2}\right) \tag{3}$$

where w_i is a weight coefficient depending on the magnitude of $\boldsymbol{e}_i$, w_0=1/3, $w_{1,\ldots,6}$=1/18, $w_{7,\ldots,18}$=1/36. It can be shown through Chapman–Enskog expansion (Chapman et al. 1960) that the NSE can be recovered from the lattice BGK model with an error proportional to $O(Ma^3)$, where $Ma = u/c_s$ is the Mach number of the system:

$$\frac{\partial\rho}{\partial t} + \nabla\cdot(\rho\boldsymbol{u}) = 0 \tag{4}$$

$$\frac{\partial(\rho\boldsymbol{u})}{\partial t} + \nabla\cdot(\rho\boldsymbol{u}\boldsymbol{u}) = -\nabla p + \nu\left(\nabla^2(\rho\boldsymbol{u}) + \nabla(\nabla\cdot(\rho\boldsymbol{u}))\right) + O(Ma^3) \tag{5}$$

Here $p = c_s^2\rho$ is the pressure, $c_s = c/\sqrt{3}$ is the speed of sound and the kinematic viscosity ν is related to the relaxation time τ by $\nu = ((2\tau-1)/6)(\Delta x^2/\Delta t)$.

2.2 Modelling temperature through a coupled model

In order to simulate the temperature, a coupled model (Guo et al. 2002) is used. In this model, the velocity and density are solved as usual using a D3Q19 lattice with a BGK collision operator and the temperature is solved on a separate, smaller, D3Q6 lattice, as shown in Fig. 1(b). When temperature is added as a separate scalar or concentration field advected by the fluid and the buoyancy effects are taken into account by adding a forcing term to the NSE, relative to the temperature differences, this is also known as the Boussinesq approximation (Tritton 1978). The six temperature distribution functions $\boldsymbol{T} = \{T_i\}$, $i \in \{1,..., 6\}$ are streamed along D3Q6 velocities and relaxed using the corresponding BGK equation:

$$T_i\left(\boldsymbol{x}+c\boldsymbol{e}_i\Delta t,\, t+\Delta t\right) = T_i\left(\boldsymbol{x},t\right) - \frac{1}{\tau_T}\left(T_i\left(\boldsymbol{x},t\right) - T_i^{(\mathrm{eq})}\left(\boldsymbol{x},t\right)\right) \tag{6}$$

Here τ_T is the relaxation time for the temperature field, T_i is the corresponding distribution function along the direction $\boldsymbol{e}_i$ and $T_i^{(\mathrm{eq})}$ is the equilibrium distribution function given by

$$T_i^{(\mathrm{eq})}\left(\boldsymbol{x},t\right) = \frac{T}{6}\left(1+2\frac{\boldsymbol{e}_i\cdot\boldsymbol{u}}{c}\right) \tag{7}$$

The fluid temperature is computed from the temperature distribution functions:

$$T = \sum_{i=1}^{6} T_i \tag{8}$$

The thermal diffusivity D of the fluid is linked to the temperature relaxation time by $D = \left(\left(2\tau_T - 1\right)/6\right)\cdot\left(\Delta x^2/\Delta t\right)$. We can again recover (Guo et al. 2002) the following macroscopic temperature equation from the temperature BGK equation:

$$\frac{\partial T}{\partial t} + \nabla\cdot\left(\boldsymbol{u}T\right) = D\nabla^2 T + O\left(Ma^2\right) \tag{9}$$

In order to take account of the buoyancy effects the two lattice Boltzmann simulations are coupled via the Boussinesq approximation (Tritton 1978) as mentioned before. With this approximation, it is assumed that all fluid properties (density, viscosity, thermal diffusivity) can be considered as constant except in the body force term, where the fluid density ρ is assumed to be a linear function of the temperature: $\rho = \rho_0\left(1-\beta\left(T-T_0\right)\right)$ where ρ_0 and T_0 are respectively the average fluid density and temperature, and β is the coefficient of thermal expansion. With the Boussinesq approximation included, Eqs. (4) and (5) become

$$\nabla\cdot\boldsymbol{u} = 0 \tag{10}$$

$$\frac{\partial\boldsymbol{u}}{\partial t} + \boldsymbol{u}\cdot\nabla\boldsymbol{u} = -\nabla p + \nu\nabla^2\boldsymbol{u} - \boldsymbol{g}\beta\left(T-T_0\right) \tag{11}$$

In the LBM formulation, the Boussinesq forcing term $\boldsymbol{F}_B = -\boldsymbol{g}\beta(T-T_0)$ is added to the right hand side of the LBGK Eq. (1):

$$f_i\left(\boldsymbol{x}+c\boldsymbol{e}_i\Delta t, t+\Delta t\right) = f_i\left(\boldsymbol{x},t\right) - \frac{1}{\tau}\left(f_i\left(\boldsymbol{x},t\right) - f_i^{(\mathrm{eq})}\left(\boldsymbol{x},t\right)\right) + F_i\Delta t \tag{12}$$

where F_i is computed using the following (Guo et al. 2002)

$$F_i = \left(1-\frac{1}{2\tau}\right)w_i\left(\frac{\boldsymbol{e}_i-\boldsymbol{u}}{c} + \frac{\left(\boldsymbol{e}_i\cdot\boldsymbol{u}\right)^2}{c^2}\boldsymbol{e}_i\right)\cdot\boldsymbol{F}_B \tag{13}$$

and the macroscopic fluid velocity $\boldsymbol{u}$ is redefined as

$$\boldsymbol{u} = \frac{1}{\rho}\left(\sum_i \boldsymbol{e}_i f_i + \frac{\Delta t}{2}\boldsymbol{F}_B\right) \tag{14}$$

2.3 Inclusion of turbulence model

Airflow in indoor environments is generally turbulent (Srebric 2010); hence our flow solver should take into account the effect of turbulence. In order to simulate turbulent flows with LBM, it is necessary to resolve a wide range of scales of fluid motion present in such flows. Resolving all the scales in a turbulent flow simulation, including the smallest ones, would require a very fine lattice and very long computation time. Instead, a Smagorinsky sub-grid/sub-lattice model similar to the traditional CFD based large eddy simulation (LES) (Smagorinsky 1963), can be used to simulate the effects of the unresolved sub-grid motion on the resolved fluid motion. In the LBM formulation, the effect of the sub-grid is incorporated into local relaxation time τ_S (Hou et al. 1996). This modified relaxation time is then used in the relaxation process, so each node of the lattice relaxes at different rates. For a more detailed discussion about sub-grid modelling in LBM see (Hou et al. 1996).

3 Performance of the LBM model

In order to assess the performance of the LBM program, two simplified models were considered, a standard lid-driven 3D cavity benchmark and airflow in an empty room.

3.1 Driven cavity benchmark

A 3D cubic cavity of height L containing an incompressible viscous fluid is modelled; the geometry is shown in Fig. 2. The fluid flow is considered to be isothermal and laminar.

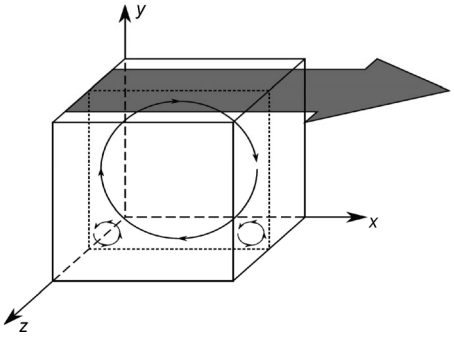

Fig. 2 Schematic diagram of 3D lid-driven cavity benchmark

It is primarily driven by the constant translation of the top lid aligned with the x-axis. The boundary condition on the top-lid is: $\boldsymbol{u}(y{=}L) = (U_{\text{lid}}, 0, 0)$ and the no-slip boundary conditions on the other walls are: $\boldsymbol{u}= (0, 0, 0)$. The popularity of this benchmark comes from its ability to generate rich flow structure while maintaining a simplified geometrical shape and boundary condition. Flow field in the lid-driven cavity has been studied extensively both experimentally (Aidun et al. 1991) and numerically (Albensoeder and Kuhlmann 2005; Ku et al. 1987).

Results presented in Fig. 3 compare the time-independent steady velocity profiles from the 3D LBM simulation at a Reynolds number of 100 and 1000 with computational results published by Ku et al. (1987) and Albensoeder and Kuhlmann (2005) respectively. Our LBM results are clearly in good agreement with the benchmark results, obtained through highly accurate spectral based CFD methodology, at both Reynolds numbers. This gives confidence in the model to apply to more complex scenarios including those representative of indoor environments.

3.2 Empty room model

The second case considered an empty ventilated room and compared results from a commercial CFD software ANSYS Fluent v13 (ANSYS 2010) based LES simulation and our 3D LBM model running on the GPU. The simulated room is based on a real 32 m^3 bioaerosol chamber (King et al. 2013) and the geometry of the room is shown in Fig. 4. Warm air is assumed to be supplied to the room through a high level wall mounted inlet on one side, at a constant speed of u_0 = 0.48 m/s normal to the inlet (equivalent to 6 air changes per hour (ACH)) and temperature of T_{in} = 22 °C. On the other side of the room there is a low level outlet with zero pressure boundary condition. The walls of the room are maintained at a temperature of T_{wall} = 15 °C. The Reynolds number of the room computed from the hydraulic diameter of the inlet was 10200 (see Table 1).

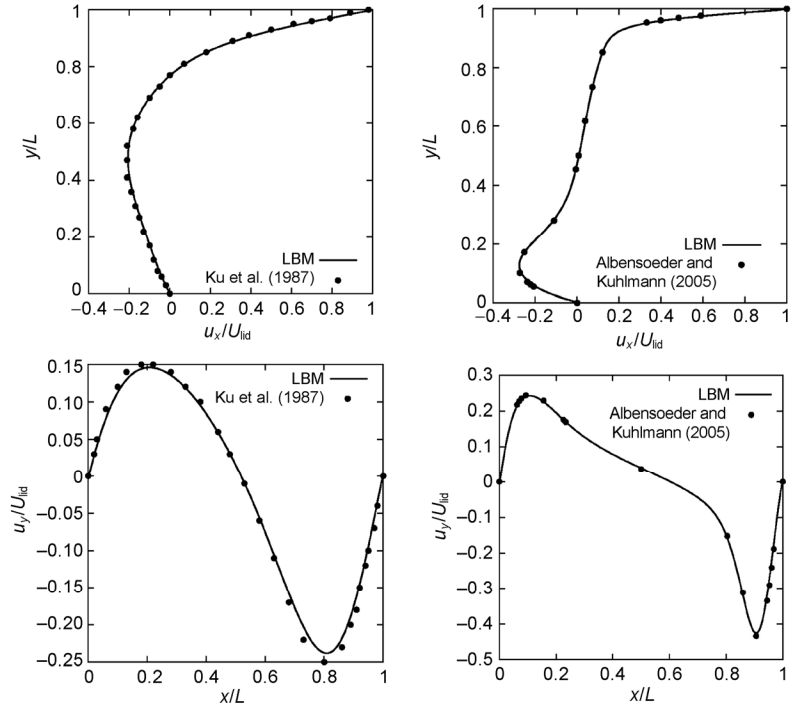

Fig. 3 Velocity profiles along x-axis (top plot) and along y-axis (bottom plot) through the geometric centre of the 3D lid-driven cavity in Fig. 2. The Reynolds number (based on the cavity height L and lid velocity U_{lid}) of the flow are Re = 100 (left plot) and Re = 1000 (right plot) with grid resolution of 256^3. The • sign represents computational results of (Ku et al. 1987) (left plot) and (Albensoeder and Kuhlmann 2005) (right plot)

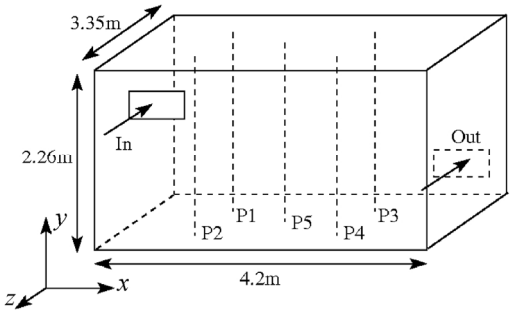

Fig. 4 Ventilated test chamber geometry showing the locations of supply and extract vents along with the position of the "poles" P1–P5 for velocity and temperature comparisons

The LBM simulation was performed on a regular mesh of 1.7 million nodes. The choice of the number of nodes in LBM was found to be a good trade-off between speed and accuracy (Delbosc et al. 2014). The speed at the inlet is 0.1 in lattice units and the viscosity is computed to match the non-dimensional Reynolds number in the test chamber (Delbosc et al. 2014). Bounce back boundary condition was imposed on the velocity distribution functions to realise no-slip velocity on the walls at the macroscopic scale (Chen and Doolen 1998). A fixed value was specified for the corresponding temperature distribution functions on the walls. Inlet and outlet conditions were implemented using the Zou He boundary condition (Chen and Doolen 1998). No near wall treatment was implemented for the current LBM based LES simulation. To compare the results of the LBM calculation we performed a large eddy simulation (LES) using ANSYS Fluent v13 (ANSYS 2010) based on the Navier–Stokes equations. This simulation was carried out on a mesh composed of 534000 hexahedral cells and refined at the inlet and outlet surfaces. Boundary conditions on the walls were no-slip for the velocity and a fixed value of 15 °C for the temperature. At the inlet a fixed velocity of 0.48 m/s was imposed and the outlet was assigned a zero pressure condition. We have used the Smagorinsky sub-grid model for turbulence modelling and the default wall functions for near wall treatment, see ANSYS Fluent user manual (ANSYS 2010). Simulation parameters for both models are set out in Table 1. In both the LES and LBM models, flow was simulated for a total of 460 seconds of physical time so that the flow inside chamber becomes statistically steady. We then averaged all the flow variables over a further 100 seconds of computation to find their mean and enable a steady-state comparison. The LES results were considered to be converged when the residuals of all the governing equations were less than 10^{-5} at every time step. The LES CFD simulation was performed on a server with 16 CPU processor cores and each physical second of simulation required 7 minutes of real computation time; total simulation time to generate the results was therefore 65 hours. The LBM simulation on a

Table 1 Computational domain and simulation parameters of ANSYS CFD and LBM method used to simulate the flow inside the test chamber in Fig. 4

Parameter	CFD (physical units)	LBM (lattice units)
Inlet velocity u_0	0.48 m/s	0.1
Inlet temperature T_{in}	22 °C	7
Reference temperature T_0	18.5 °C	3.5
Wall temperature T_{wall}	15 °C	0
Fluid density ρ	1.225 kg/m^3	1.0
Prandtl number Pr	0.75	0.75
Kinematic viscosity ν	1.46×10^{-5} m^2/s	1.049×10^{-6}
Thermal diffusivity D	1.963×10^{-5} m^2/s	1.40×10^{-6}
Room height (H)	2.26 m	86
Room width (W)	3.36 m	127
Room length (L)	4.20 m	160
Inlet height (h)	0.23 m	9
Inlet width (w)	0.48 m	18
Reynolds number $Re = 4(h \times w)/2(h + w)$	10200	
Sub-grid Smagorinsky model constant Cs	0.1	0.04
Turbulent Prandtl number Pr_t	0.85	0.85
Number of grid points	$106 \times 58 \times 85$ with inlet & outlet refinement = 533918	$160 \times 86 \times 127 = 1.7 \times 10^6$ Uniform cubic.
Time step	0.01 s	1

single Tesla K40 (NVIDIA 2013) GPU took 0.34 seconds to compute a physical second of simulation time.

Figure 5 shows a comparison between the LES and LBM models during the initial transient phase of the simulation of an isothermal turbulent airflow in the test chamber of Fig. 4. The images show contours of instantaneous velocity magnitudes at various times (0.5 to 5.5 seconds) on a plane through the centerline of the inlet. The inlet airflow is inclined at angle with the inlet centerline. Our LBM simulation shows qualitatively similar behaviour to the LES simulation. The main difference is the appearance of the pressure waves as shocks in the LBM velocity field during the initial phase of the simulation due to slightly compressible formulation of the LBM algorithm (Chen and Doolen 1998).

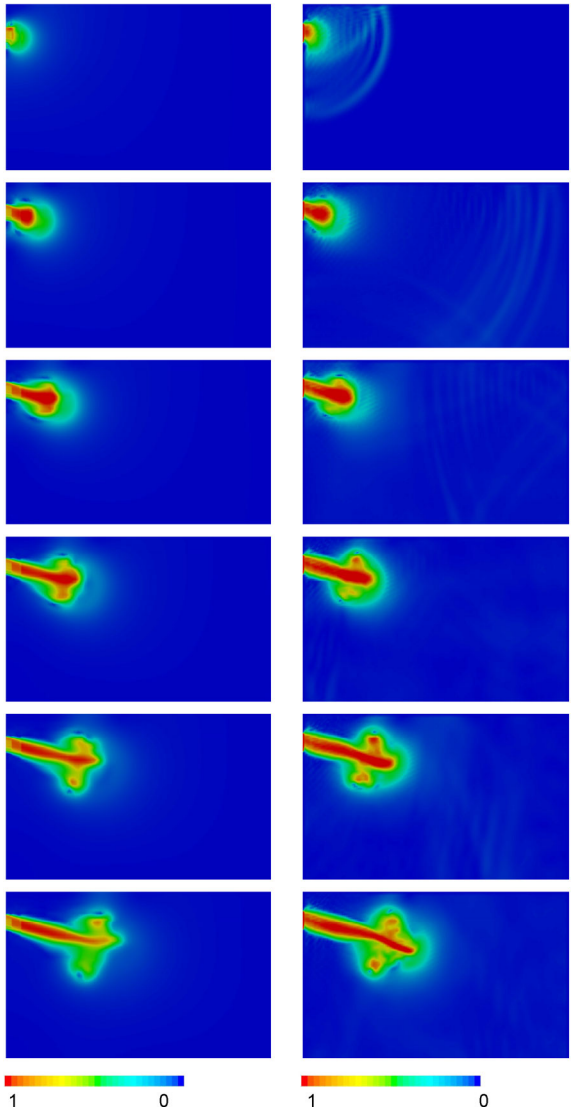

Fig. 5 Transient comparison of the isothermal normalised velocity magnitude $|\boldsymbol{u}|$ of the inlet jet of the test chamber shown in Fig. 4: FLUENT simulation (left plots)and LBM results (right plots). From top to bottom the images show snapshots at times 0.5,1.5, 2.5, 3.5, 4.5 and 5.5 seconds respectively

Figure 6 shows the normalised contour plots of the time averaged velocity magnitude and temperature respectively across a plane through the centreline of the chamber inlet. In both cases the contours show the effect of buoyancy on the incoming airflow. The warm inlet jet rises and comes in contact with the cold ceiling and drops towards the floor as it reaches the other end of the chamber. This creates a vertically stratified flow pattern captured both by LES and LBM simulations. The boundary layer produced by LBM simulation appears to be thicker than that produced by LES simulation. This difference could be due to the absence of any near wall modelling in the current LBM implementation and also due to the type of microscopic boundary used to realise the equivalent macroscopic no-slip boundary conditions (Chen and Doolen 1998). A detailed discussion on the various types of LBM boundary conditions and their limitations are given in (Delbosc et al. 2014) and references therein. Figure 7 compares the profiles of the mean velocity and temperature computed along the chamber height at five different positions designated as poles P1–P5 inside the chamber (see Fig. 4). The position coordinates (in meters) of the poles P1–P5 on the floor (x-z plane) of the chamber are (1.1, 0, 1), (1.1, 0, 2.36), (3.1, 0, 1), (3.1, 0, 2.36) and (2.1, 0, 1.68) respectively. Our LBM results show similar trends to the LES model but differ numerically especially for the temperature profiles near the top wall of the chamber. This discrepancy could be due to the absence of any sub-grid forcing term due to temperature gradients (Delbosc et al. 2014), absence of near wall modelling and also due to the choice of temperature microscopic boundary conditions. We are currently working on the implementation of an improved LBM model to address some of these issues of our model.

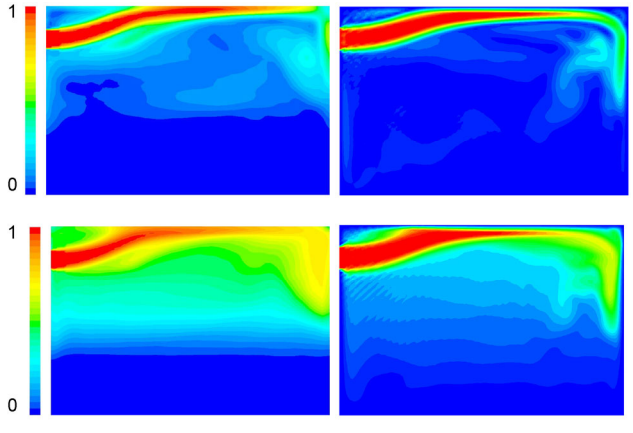

Fig. 6 Steady-state comparison between LES (left plots) and LBM simulation (right plots) of the test chamber (Fig. 4). Contours of normalised mean velocity magnitude $|\boldsymbol{u}|$ (top plots) and mean temperature T (bottom plots) averaged over 100 seconds are shown across the plane through the centerline of the chamber inlet

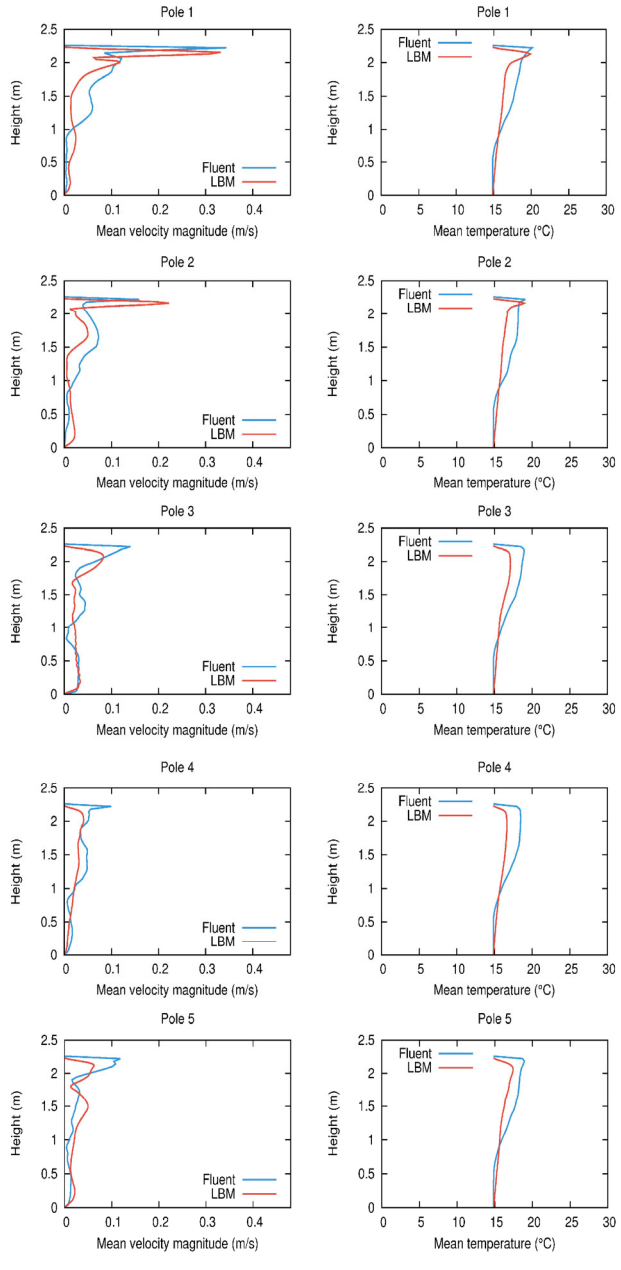

Fig. 7 Comparison between LBM and LES simulation of the test chamber (Fig. 4). Mean velocity magnitude (left plots) and mean temperature (right plots) profiles along the y-axis at positions P1 to P5 (top to bottom) respectively

3.3 Real-time performance

In order to simulate fluid flow in real-time (or faster than real-time), the physical time between two simulation-steps needs to be equal to (or bigger than) the time taken by the computer to simulate one time-step. In order to compute the physical time corresponding to one simulation time-step, we need to convert the "lattice-units" used in our program into "real-world units" (Delbosc et al. 2014). To do this, the physical quantities are rescaled into dimensionless quantities through conversion factors: we will write $C_{phys} = Q_C\, C_{LBM}$, where C_{phys} is the physical quantity, Q_C is the conversion factor and C_{LBM} is the dimensionless quantity used in the LBM. If we consider length, time and speed in our simulation, only two of them can be independently scaled using the conversion factors and the third one can be obtained from a combination of these two. We can write the scaling of the length, time and speed as: $x_{phys} = Q_x x_{LBM}$, $t_{phys} = Q_t\, t_{LBM}$ and $u_{phys} = Q_u\, u_{LBM}$. If we assume length and speed to be independently scaled the scaling factor Q_t for the time can be found from $Q_t = Q_x/Q_u$. The velocity conversion factor can be computed from the characteristic lattice velocity u_{LBM} and the characteristic physical velocity u_{phys}. The lattice velocity u_{LBM} should never exceed 0.2 due to stability (Delbosc et al. 2014). In the case of the chamber (see Fig. 4) the velocity conversion factor is based on the inlet speed and it is given by $Q_u = u_{phys}/u_{LBM} = 0.48/0.1 = 4.8$ m/s. The length conversion factor is based on the chamber width 3.36 m and the number of nodes (127) along that direction, hence $Q_x = 3.36\text{m}/127 = 0.026$ m. Finally the physical time between two time steps in our LBM simulation is calculated to be $\Delta t = Q_t = Q_x/Q_u = 0.0055$ seconds. To compute the speed-up the physical time needs to be compared to the computational time. The flow in the test chamber can be simulated at rate which is equivalent to the room made of 1.7 million nodes being updated 540 times per second, so each time-step is computed in 1.85×10^{-3} seconds. Computing the ratio to the physical time shows that a speed-up of 2.97 is obtained. Thus, the airflow in this room can be simulated 2.97 times faster than the real flow.

4 Application to a hospital room

The LBM model was applied to a hypothetical four-bed hospital room scenario to explore the potential insights that can be derived from a real-time transient model. Figure 8(a) shows the geometry of this scenario. The room is assumed to be ventilated via a supply inlet mounted on the left hand wall and air is extracted by a similar vent on the opposite wall. Both the inlet and the extract vents are assumed to be simple rectangular (0.48 m × 0.23 m) openings without any grills. The room (7.2 m × 7.2 m × 3 m) contains patients (1.0 m × 0.3 m × 0.3 m) on four beds (1.8 m × 0.6 m × 0.75 m) and a healthcare worker (HCW) of similar dimensions as the patients positioned at the center of the room. The positions of the inlet and outlet vents are on the lower left and higher right wall respectively. The inlet air temperature was fixed at 15 °C and the patients and HCW were represented by heat sources with a fixed temparature of 37 °C similar to human body temperature. All the walls including the floor, ceiling and beds of the ward are assumed to be thermally insulated with zero air velocity conditions imposed on them. Figure 8(b) shows snapshots (volume render) of the time dependent

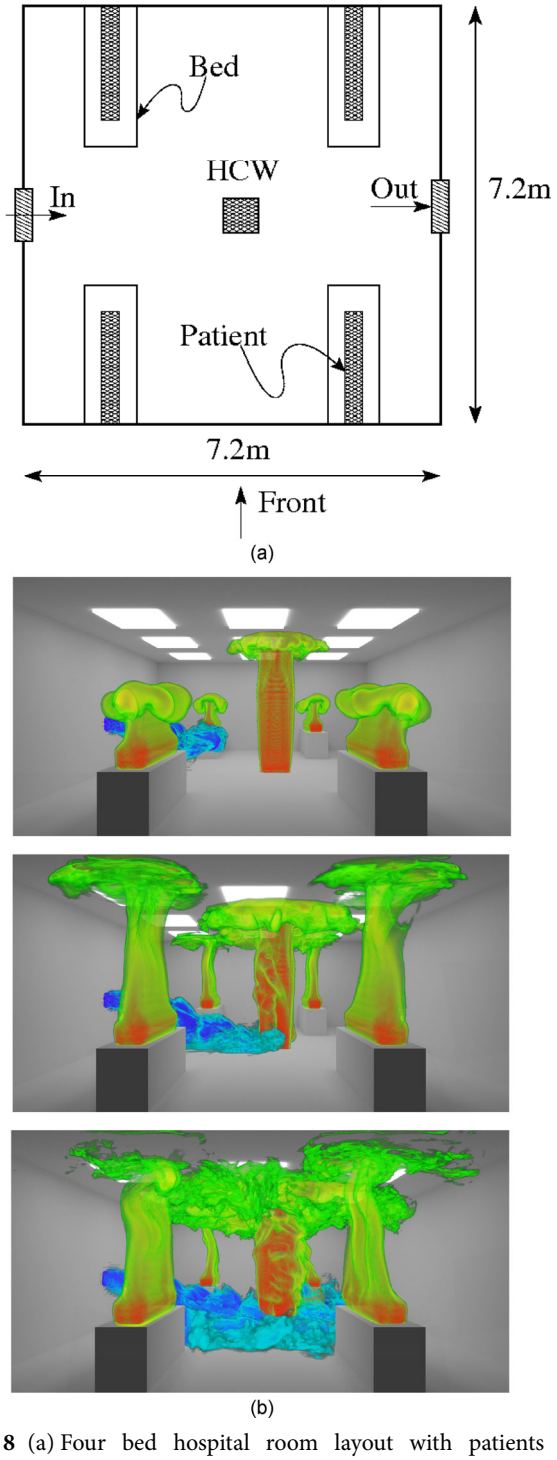

Fig. 8 (a) Four bed hospital room layout with patients and healthcare worker (HCW). (b) Front view of the LBM simulation of the ward, where the color corresponds to temperature distribution in the ward. Red corresponds to hot (37 °C) and blue cold (15 °C). The three images (top to bottom) in (b) corresponds to three time-ordered snapshots at times 4, 10 and 20 seconds respectively of the evolving turbulent temperature field

turbulent flow field inside the room. The images were rendered offline using Blender (Blender 2010) to add lighting and realism. The colours represent temperature field inside the ward (see Fig. 8(b)). The images in Fig. 8(b) shows the complex interactions between the cold inlet airflow and the thermal plumes of the patients and the HCW. Positions of the inlet, outlet and the HCW could be interactively changed while the simulation is running, providing an unprecedented level of visual and quantitative feedback into the effects of different ventilation strategy on thermal comfort and IAQ. Furthermore it can also provide a quick and visual insight into the effects of ward design and user behaviour on thermal comfort, IAQ and potentially airborne infection risk in a ward.

5 Discussions and conclusions

A novel LBM based interactive real-time CFD technique with integrated visualisation method has been implemented on the graphics processor unit (GPU). Simulations on an empty test chamber and a hypothetical hospital room have shown the capability of the LBM method to reproduce realistic results which compare well with traditional CFD based methodology. The computational results were validated against mechanically driven 3D cavities and a 32 m^3 ventilated test chamber. The results of these simulations are compared with both benchmark results in the literature and simulations using standard LES approaches, showing reasonable agreement and faster computational time. Adding a dynamic sub-grid model and implementing wall functions in LBM which will be done in the future should capture the wall boundary layers more accurately. Since our algorithm is mainly dominated by GPU memory bandwidth (Thibault and Senocak 2009) adding more computations will not degrade the real-time capability of our method. Furthermore implementation of non-uniform lattice and extending the algorithm to multiple-GPU platform will enable real-time simulation of indoor environments with complicated geometry and large domain sizes.

Experimental validation of LBM based methods exists in the literature for simple configurations (Ampofo 2003; Zhang and Lin 2010). But in a realistic environment where the flow field is transient and turbulent it is difficult to obtain the data and often becomes less detailed and less reliable in terms of quality for validation. We hope to perform a detailed chamber based experiments in the future for the purpose of validating our computational results.

Our LBM based method has the potential for accelerating the performance based design optimisation procedure of building ventilation system during the design phase, as well as allowing real-time control and prediction for building management systems. A potential field of application is real-time simulation of airborne pollutant transport, for example in hospitals, enabling smart and intelligent response to the spread of contaminants.

Acknowledgments

This work was carried out as part of a Ph.D. studentship supported by the Schools of Civil Engineering and Mechanical Engineering, University of Leeds. The authors MAIK and CJN would like to acknowledge the support of the Engineering and Physical Sciences Research Council (EPSRC) for funding this work. We also gratefully acknowledge the support of NVIDIA Corporation with the donation of the Tesla K40 GPU used for this research.

References

Aidun CK, Triantafillopoulos NG, Benson JD (1991). Global stability of a lid-driven cavity with throughflow: Flow visualization studies. *Physics of Fluids A: Fluid Dynamics*, 3: 2081.

Albensoeder S, Kuhlmann HC (2005). Accurate three-dimensional lid-driven cavity flow. *Journal of Computational Physics*, 206: 536–558.

Ampofo F (2003). Experimental benchmark data for turbulent natural convection in an air filled square cavity. *International Journal of Heat and Mass Transfer*, 46: 3551–3572.

ANSYS (2010). ANSYS Academic Research, Release 13, Help System, FLUENT User's Guide. ANSYS Inc.

Asfour OS, Gadi MB (2007). A comparison between CFD and Network models for predicting wind-driven ventilation in buildings. *Building and Environment*, 42: 4079–4085.

Béghein C, Jiang Y, Chen QY (2005). Using large eddy simulation to study particle motions in a room. *Indoor Air*, 15: 281–290.

Bhatnagar PL, Gross EP, Krook M (1954). A model for collision processes in gases. I. Small amplitude processes in charged and neutral one-component systems. *Physical Review*, 94: 511–525.

Blender (2010). Blender v2.5—A 3D modeling and rendering package. Blender Institute, Amsterdam. Available at http://www.blender.org.

Chapman S, Burnett D, Cowling T (1960). The Mathematical Theory of Non-uniform Gases. Cambridge: Cambridge University Press.

Chen S, Doolen GD (1998). Lattice Boltzmann method for fluid flows. *Annual Review of Fluid Mechanics*, 30: 329–364.

Crouse B, Krafczyk M, Kühner S, Rank E, van Treeck C (2002). Indoor air flow analysis based on lattice Boltzmann methods. *Energy and Buildings*, 34: 941–949.

Delbosc N, Summers JL, Khan AI, Kapur N, Noakes CJ (2014). Optimized implementation of the Lattice Boltzmann Method on a graphics processing unit towards real-time fluid simulation. *Computers & Mathematics with Applications*, 67: 462–475.

Elhadidi B, Khalifa HE (2013). Comparison of coarse grid lattice Boltzmann and Navier Stokes for real time flow simulations in rooms. *Building Simulation*, 6: 183–194.

Frisch U, Hasslacher B, Pomeau Y (1986). Lattice-gas automata for the Navier–Stokes equation. *Physical Review Letters*, 56: 1505–1508.

Guo Z, Shi B, Zheng C (2002). A coupled lattice BGK model for the Boussinesq equations. *International Journal for Numerical Methods in Fluids*, 39: 325–342.

Hou S, Sterling J, Chen S, Doolen GD (1996). A lattice Boltzmann subgrid model for high reynolds number flows. In: Lawniczak AT, Kapral R (eds.), Pattern Formation and Lattice Gas Automata, American Mathematical Society, pp. 151–166.

Jin M, Zuo W, Chen Q (2012). Improvements of fast fluid dynamics for simulating air flow in buildings. *Numerical Heat Transfer, Part B: Fundamentals*, 62: 419–438.

King MF, Noakes CJ, Sleigh PA, Camargo-Valero MA (2013). Bioaerosol deposition in single and two-bed hospital rooms: A numerical and experimental study. *Building and Environment*, 59: 436–447.

Ku HC, Hirsh RS, Taylor TD (1987). A pseudospectral method for solution of the three-dimensional incompressible Navier–Stokes equations. *Journal of Computational Physics*, 70: 439–462.

Mariani VC, da Silva A (2007). Natural convection: Analysis of partially open enclosures with an internal heated source. *Numerical Heat Transfer, Part A: Applications*, 52: 595–619.

Megri AC, Haghighat F (2007). Zonal modeling for simulating indoor environment of buildings: Review, recent developments, and applications. *HVAC&R Research*, 13: 887–905.

Noakes CJJ, Sleigh PA, Escombe AR, Beggs CB (2006). Use of CFD analysis in modifying a TB ward in Lima, Peru. *Indoor and Built Environment*, 15: 41–47.

NVIDIA (2013). Tesla K40 Specification. Available at http://www.nvidia.com/object/tesla_product_literature.html.

Obrecht C, Kuznik F, Tourancheau B, Roux J-J (2012). The TheLMA project: A thermal lattice Boltzmann solver for the GPU. *Computers & Fluids*, 54: 118–126.

Qin TX, Guo YC, Chan CK, Lin WY (2009). Numerical simulation of the spread of smoke in an atrium under fire scenario. *Building and Environment*, 44: 56–65.

Smagorinsky J (1963). General circulation experiments with the primitive equations. *Monthly Weather Review*, 91: 99–164.

Srebric J (2010). Editorial: Computational fluid dynamics (CFD) challenges in simulating building airflows. *HVAC&R Research*, 16: 729–730.

Stam J (1999). Stable fluids. In: Proceedings of 26th Computer Graphics and Interactive Techniques. New York, USA, pp. 121–128.

Thibault JC, Senocak I (2009). CUDA implementation of a Navier–Stokes Solver on multi-GPU desktop platforms for incompressible flows. In: 47th AIAA Aerospace Sciences Meeting, Orlando, USA.

Tritton DJ (1978). Physical Fluid Dynamics, 2nd edn. Oxford: Oxford University Press.

Wang L, Chen Q (2007). Validation of a coupled multizone-CFD Program for building airflow and contaminant transport simulations. *HVAC&R Research*, 13: 267–281.

Zhai Z (2006). Application of Computational fluid dynamics in building design: Aspects and trends. *Indoor and Built Environment*, 15: 305–313.

Zhang SJ, Lin CX (2010). Application of lattice Boltzmann method in indoor airflow simulation. *HVAC&R Research*, 16: 825–841.

Zhao B, Guan P (2007). Modeling particle dispersion in personalized ventilated room. *Building and Environment*, 42: 1099–1109.

Zuo W, Chen Q (2009). Real-time or faster-than-real-time simulation of airflow in buildings. *Indoor Air*, 19: 33–44.

Zuo W, Chen Q (2010). Fast and informative flow simulations in a building by using fast fluid dynamics model on graphics processing unit. *Building and Environment*, 45: 747–757.

Zuo W, Hu J, Chen Q (2010). Improvements in FFD modeling by using different numerical schemes, *Numerical Heat Transfer, Part B: Fundamentals*, 58: 1–16.